Supporting Information for:

Layered Perovskite $(CH_3NH_3)_2Pb(SCN)_2I_2$ Single Crystals: Phase Transition and Moisture Stability

Yangyang Dang *†‡ Guokui Liu,§ Jiewu Song, † Lingqiang Meng, ¶ Yajing Sun, ‡ Wenping Hu ‡ and Xutang Tao*†

†State Key Laboratory of Crystal Materials & Institute of Crystal Materials, Shandong University, No. 27 Shanda South Road, Jinan, 250100, P. R. China.

‡Tianjin Key Laboratory of Molecular Optoelectronic Sciences & Department of Chemistry, School of Sciences, & Collaborative Innovation Center of Chemical Science and Engineering, Tianjin University, Tianjin, 300072, P. R. China.

§School of Chemistry and Chemical Engineering, Linyi University, Linyi, 276000, P. R. China.

¶ Materials Interfaces Center, Shenzhen Institutes of Advanced Technology, Chinese Academy of Sciences, Shenzhen 518055, P.R. China.

Corresponding Author

*(Y. D.) Email: yeung_dang@tju.edu.cn

*(X. T.) Email: txt@sdu.edu.cn

EXPERIMENTAL METHODS

Figure S1. Photo and powder XRD diffractions of $Pb(SCN)_2$ powders obtained from the synthesis of $Pb(CH_3COO)_2.3H_2O$ and NaSCN, indicating the impurities of NaSCN.

Figure S2. (**a-b**) Photo and powder XRD diffractions of pure $Pb(SCN)_2$ powders obtained from the synthesis of $Pb(BF_4)_2$ and NaSCN, indicating the pure phase $Pb(SCN)_2$; (**c-d**) Photo and powder XRD diffractions of $MA_2Pb(SCN)_2I_2$ single crystal obtained by slow evaporaition method using THF solvent.

Figure S3. The crystal structure of $Pb(SCN)_2$ along the [001] direction obtained by THF or DMF solvent.

Figure S4. (a) The yellow transparent solution obtained by as-synthesized MAI and $Pb(SCN)_2$; (b) The turbid solution using the commercialized counterparts of MAI and $Pb(SCN)_2$

Figure S5 (**a**) UV-vis absorption spectra of $MA_2Pb(SCN)_2I_2$ single-crystalline powder samples obtained by different crystal growth methods; (**b**) Band gap of $MA_2Pb(SCN)_2I_2$ single-crystalline powder samples obtained by different crystal growth methods, inset: direct band gap of 2.1 eV and indirect band gap of 1.97~1.99 eV; (**c**) PL spectra of $MA_2Pb(SCN)_2I_2$ single-crystalline powder samples obtained by different crystal growth methods under 420 nm irradiation condition.

Figure S6. Crystal structural units of $(CH_3NH_3)_2Pb(SCN)_2I_2$ at 190 K and 293 K

Figure S7. (**a**) $Pb(SCN)_2I_4$ unit of $MA_2Pb(SCN)_2I_2$ at 293 K; (**b**) $Pb(SCN)_2I_4$ unit of $MA_2Pb(SCN)_2I_2$ at 363 K

Figure S8. High temperature phase transition processes of $MA_2Pb(SCN)_2I_2$ powders by mechanical mixing method, corresponding to the powder XRD patterns

Figure S9. PXRD patterns of $MA_2Pb(SCN)_2I_2$ single-crystalline samples during melting and solidification processes in inert and air atmosphere.

Figure S10. The phase transition processes of $MA_2Pb(SCN)_2I_2$ thin film at high temperature

Figure S11. The detailed phase transition processes of $MA_2Pb(SCN)_2I_2$ thin film at high temperature

Figure S12. Stability and powder XRD patterns of $MA_2Pb(SCN)_2I_2$ single-crystalline samples at different conditions (air, light illumination, vacuum and moisture)

Figure S13. Core level XPS spectra for $MA_2Pb(SCN)_2I_2$ single crystal obtained by fresh synthesized and place in air for a long time. (**a**) XPS survey; (**b**) S 2p, (**c**) I 3d, (**d**) Pb 4f, (**e**) C 1s and (**f**) N 1s

Figure S14. Transformation processes of $MAPbI_3$ single-crystalline grinding powder samples immersing in H_2O and then heating to 90 ^oC and cooling down to room temperature in air, which was verified to be $MAPbI_3$ and PbI_2 mixtures

Table S1. Crystal data and structure refinements for $Pb(SCN)_2$ and $MA_2Pb(SCN)_2I_2$ at 293(2)K

Table S2. Crystal data and structure refinements for $MA_2Pb(SCN)_2I_2$ at 293(2)K.

Table S3. Crystal data and structure refinements for $MA_2Pb(SCN)_2I_2$ at 190 K and 363 K

Table S4. Crystal data and structure refinements for $MAPbI_3$ and $MA_2Pb(SCN)_2I_2$ obtained when exposed to H_2O and then heating to 90 ^oC and cooling down to room temperature in air.

Movie S1. The phase transition processes of $MA_2Pb(SCN)_2I_2$ powders in ambient atmosphere.

Movie S2. The phase transition processes of $MA_2Pb(SCN)_2I_2$ thin films in ambient atmosphere.

EXPERIMENTAL METHODS

Single-crystal and Powder X-ray Diffraction Studies. $MA_2Pb(SCN)_2I_2$ single-crystalline powders were measured using a *Bruker-AXS D8 ADVANCE X-Ray* diffractometer with Cu-Kα_1 radiation (λ= 1.54186 Å) in the range of 10°-80° (2θ), which was also depicted elsewhere.[1-5] The suitable crystals of $MA_2Pb(SCN)_2I_2$ were selected and fixed on a *SuperNova*, Dual, Cu at zero, *AtlasS2* diffractometer. The crystal was kept at 190 K, 293(2) K and 363 K during data collection. Using *Olex2*,[6] the structure was solved with the *ShelXS*[7] structure solution program using direct methods and refined with the *ShelXL*[8] refinement package using Least Squares minimization.

Thermogravimetric Analysis (TGA) and Differential Scan Calorimetry (DSC) Measurements. Differential scanning calorimetry (DSC) and thermogravimetric analysis (TGA) were carried out using a TGA/DSC1/1600HT analyzer (*METTLER TOLEDO* Instruments). $MA_2Pb(SCN)_2I_2$ samples were placed in a platinum crucible, and heated at a rate of 10 °C min^{-1} from room temperature to 800 °C under flowing nitrogen gas. Differential Scan calorimetry (DSC) measurements were performed on Polyma Instruments (DSC-200-F3 Maia). $MA_2Pb(SCN)_2I_2$ powder samples were placed in a platinum crucible, and heated at a rate of 10 °C min^{-1} from room temperature to 127 °C, and then cooled to -93 °C in liquid N_2 atmosphere and shifted back to room temperature under flowing N_2 gas.

UV-vis-NIR diffuse reflectance spectra measurements. UV-vis-NIR diffuse reflectance spectroscopy was carried out using a Varian Cary 5000 spectrophotometer equipped with an integrating sphere over the spectral range 300-800 nm. $MA_2Pb(SCN)_2I_2$ single crystals were grinded into single-crystalline powders. A $BaSO_4$ plate was used as the standard (100% reflectance). The absorption spectrum was calculated from the reflectance spectrum using the Kubelka-Munk function: $\alpha/S = (1-R)^2/(2R)$,[9] where α is the absorption coefficient, *S* is the scattering coefficient, and R is the reflectance.

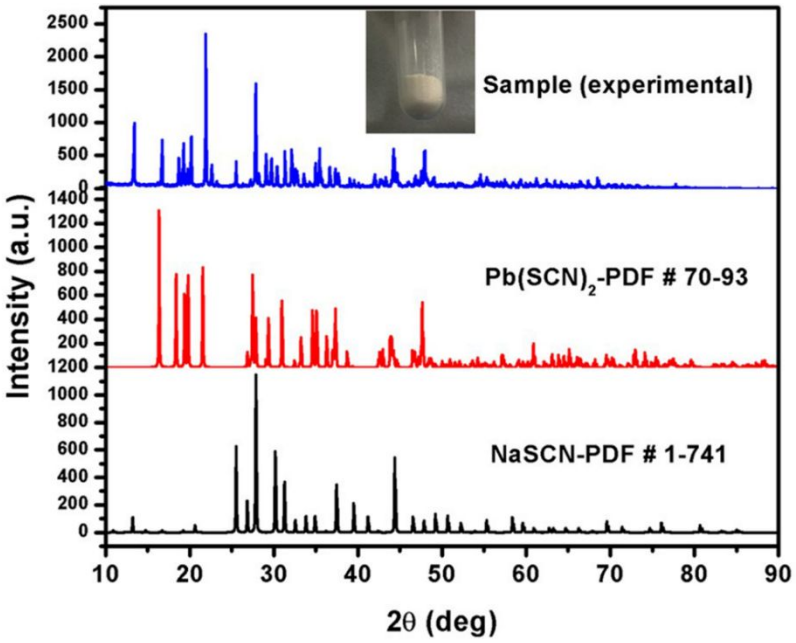

Figure S1. Photo and powder XRD diffractions of $Pb(SCN)_2$ powders obtained from the synthesis of $Pb(CH_3COO)_2.3H_2O$ and NaSCN, indicating the impurities of NaSCN.

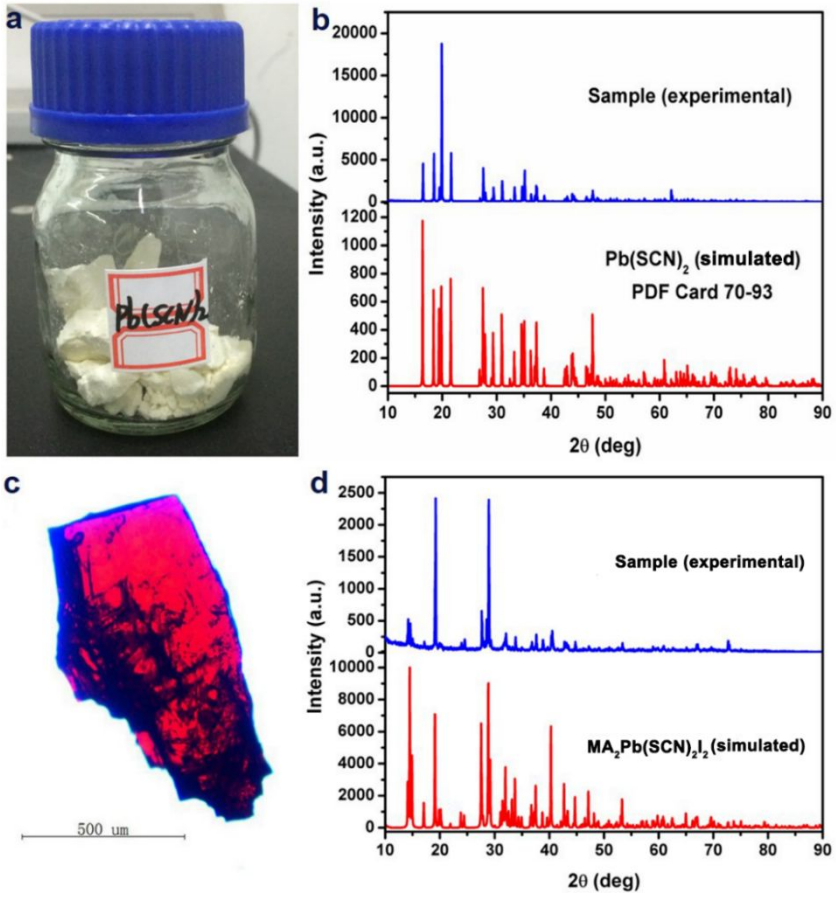

Figure S2. (**a-b**) The photo and powder XRD diffractions of pure $Pb(SCN)_2$ powders obtained from the synthesis of $Pb(BF_4)_2$ and NaSCN, indicating the pure phase $Pb(SCN)_2$; (**c-d**) The photo and powder XRD diffractions of $MA_2Pb(SCN)_2I_2$ single crystal obtained by slow evaporation method using THF solvent.

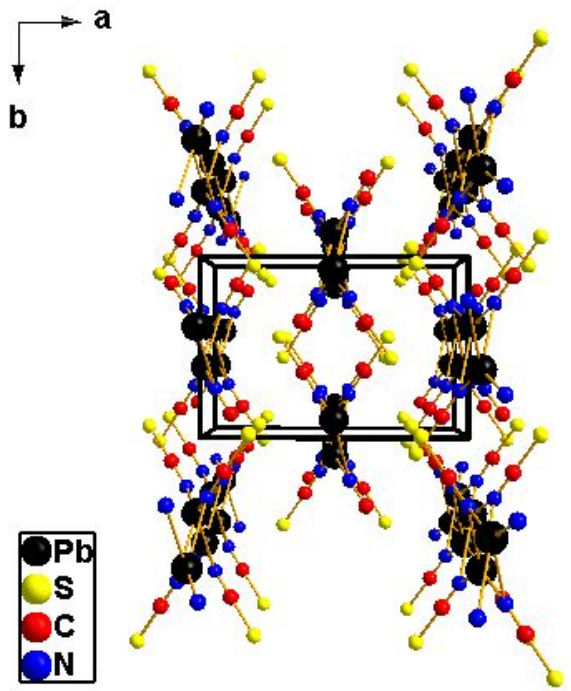

Figure S3. The crystal structure of $Pb(SCN)_2$ along the [001] direction obtained by THF or DMF solvent.

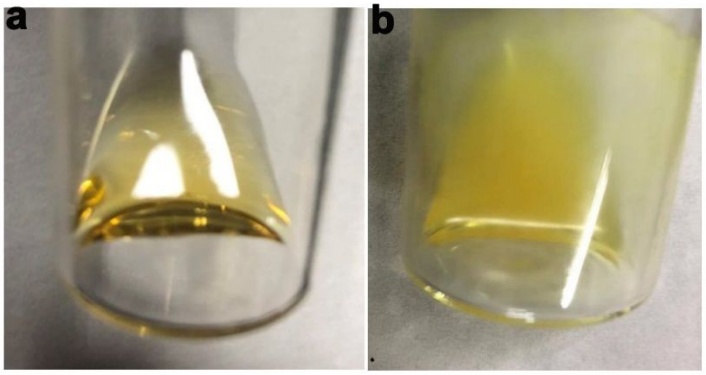

Figure S4. (a) The yellow transparent solution obtained by as-synthesized MAI and $Pb(SCN)_2$; (b) The turbid solution using the commercialized counterparts of MAI and $Pb(SCN)_2$

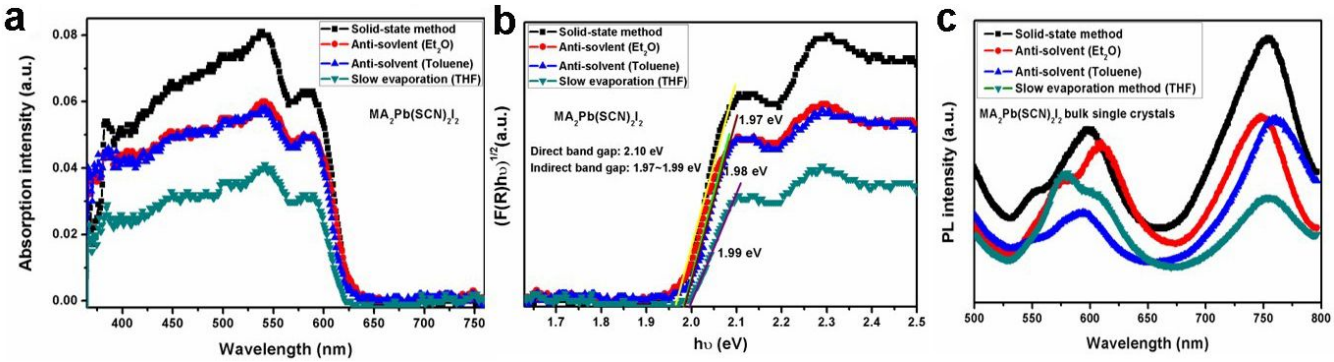

Figure S5 (**a**) UV-vis absorption spectra of $MA_2Pb(SCN)_2I_2$ grinding powder samples obtained by different crystal growth methods; (**b**) Band gap of $MA_2Pb(SCN)_2I_2$ grinding powder samples obtained by different crystal growth methods, inset: direct band gap of 2.1 eV and indirect band gap of 1.97~1.99 eV;

(**c**) PL spectra of $MA_2Pb(SCN)_2I_2$ grinding powder samples obtained by different crystal growth methods under 420 nm irradiation condition.

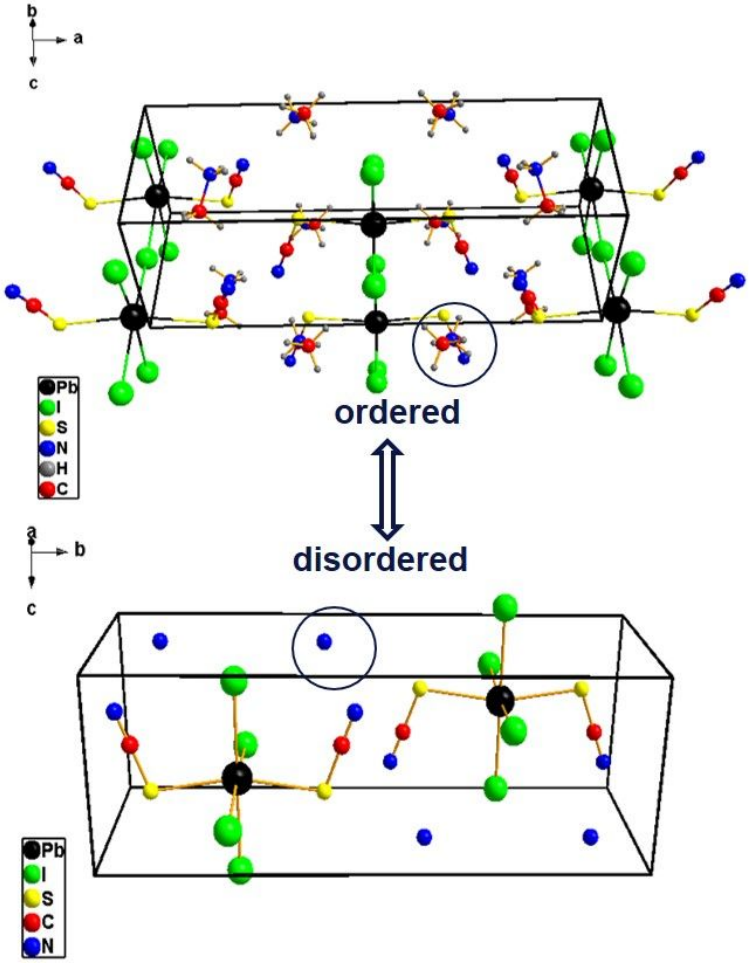

Figure S6. The crystal structural units of $(CH_3NH_3)_2Pb(SCN)_2I_2$ at 190 K and 293 K

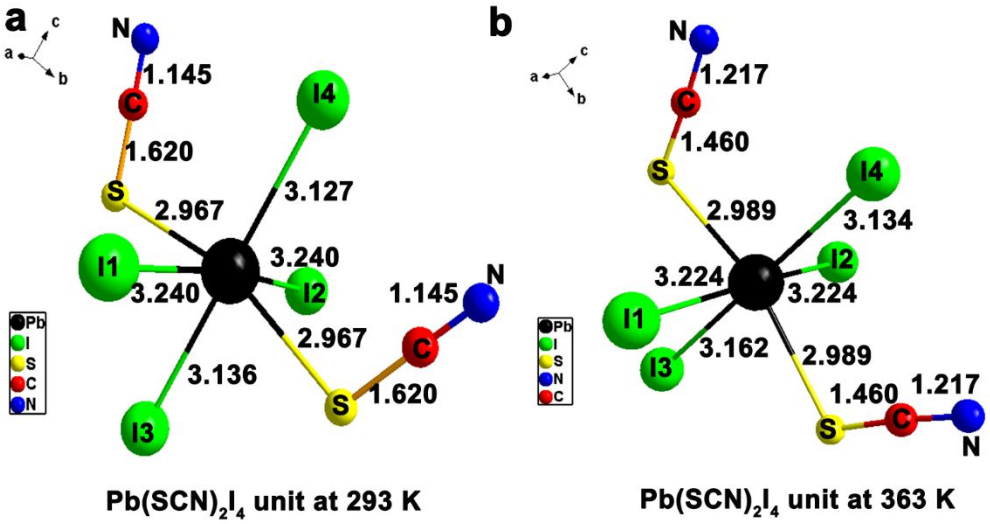

Figure S7. (**a**) $Pb(SCN)_2I_4$ unit of $MA_2Pb(SCN)_2I_2$ at 293 K; (**b**) $Pb(SCN)_2I_4$ unit of $MA_2Pb(SCN)_2I_2$ at 363 K

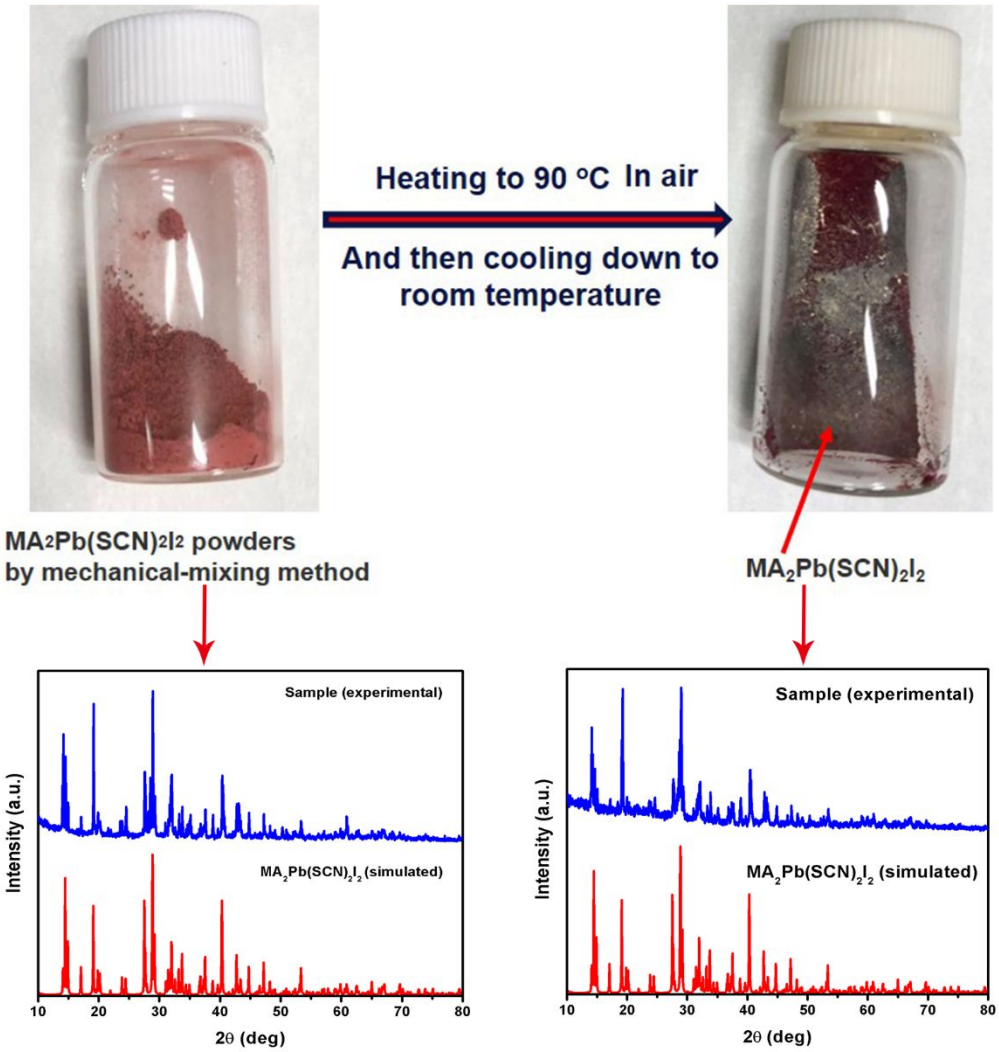

Figure S8. The high temperature phase transition processes of $MA_2Pb(SCN)_2I_2$ powders by mechanical mixing method, corresponding to the powder XRD patterns

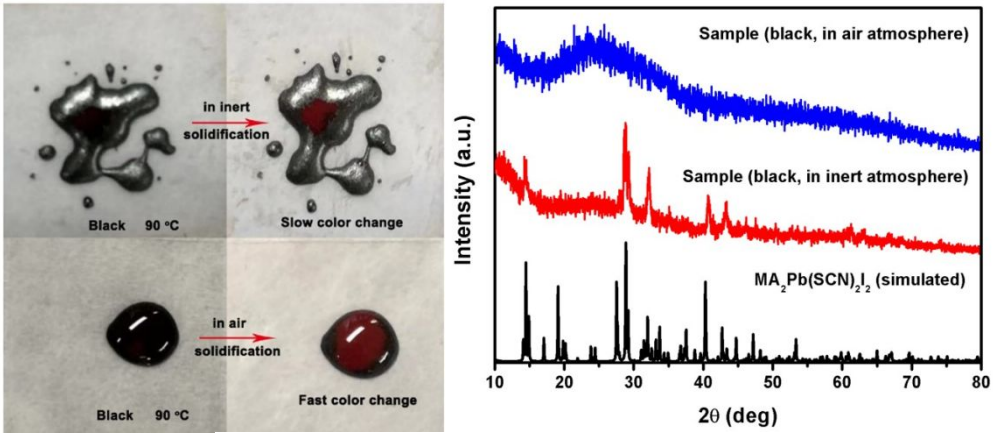

Figure S9. PXRD patterns of $MA_2Pb(SCN)_2I_2$ single-crystalline samples during melting and solidification processes in inert and air atmosphere.

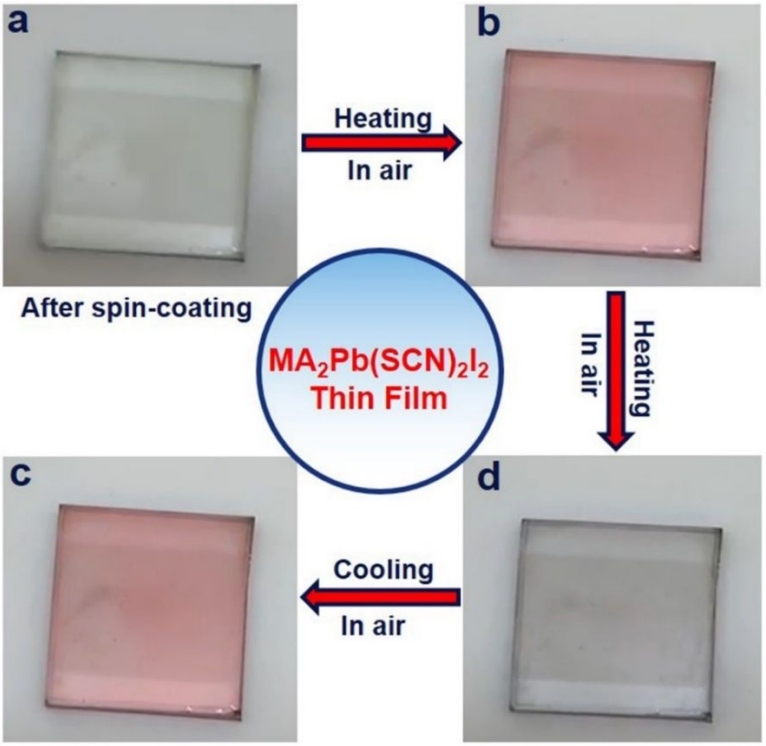

Figure S10. The phase transition processes of $MA_2Pb(SCN)_2I_2$ thin film at higher temperature(90 ^oC).

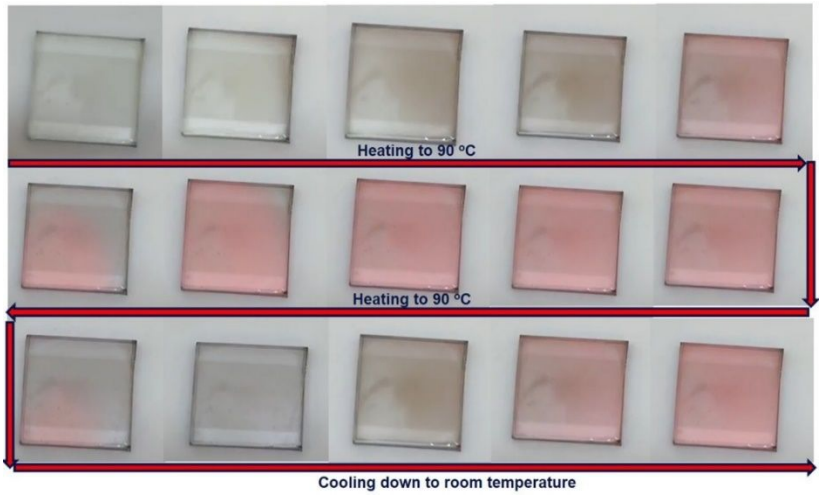

Figure S11. The detailed phase transition processes of $MA_2Pb(SCN)_2I_2$ thin film at high temperature

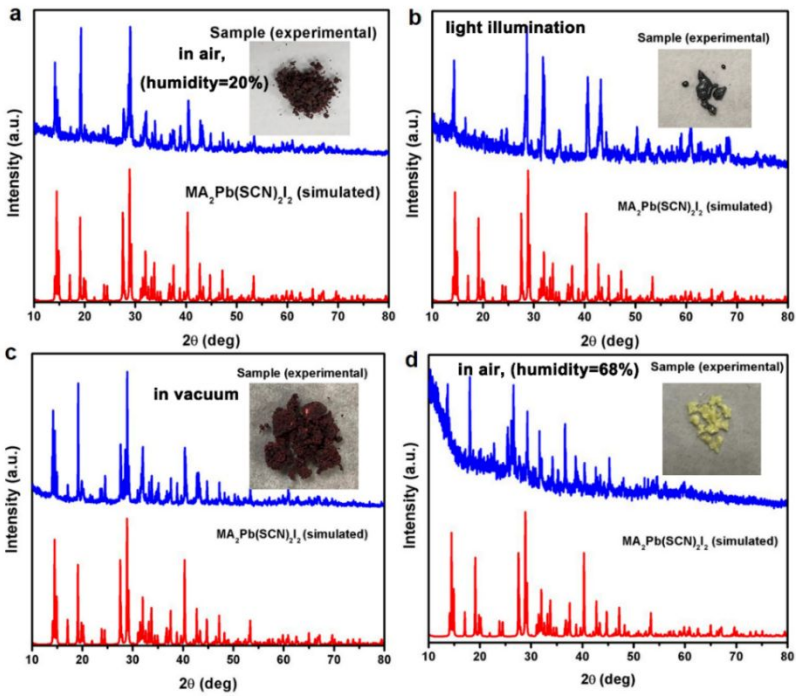

Figure S12. Stability and powder XRD patterns of $MA_2Pb(SCN)_2I_2$ single-crystalline samples at different conditions (air, light illumination, vacuum and moisture)

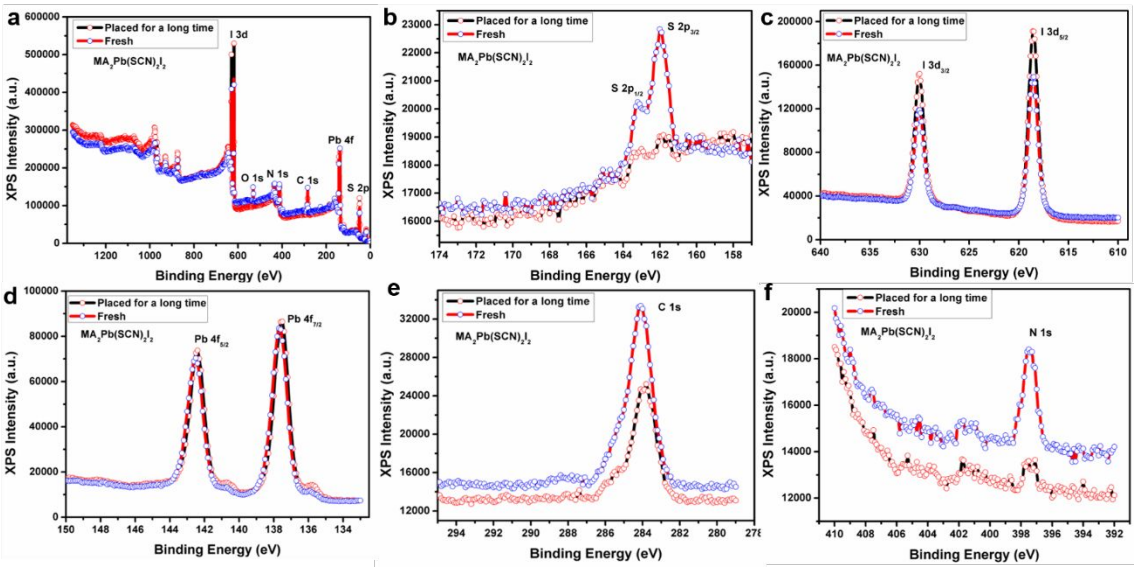

Figure S13. Core level XPS spectra for $MA_2Pb(SCN)_2I_2$ single crystal obtained by fresh synthesized and place in air for a long time, (**a**) XPS survey; (**b**) S 2p, (**c**) I 3d, (**d**) Pb 4f, (**e**) C 1s and (**f**) N 1s.

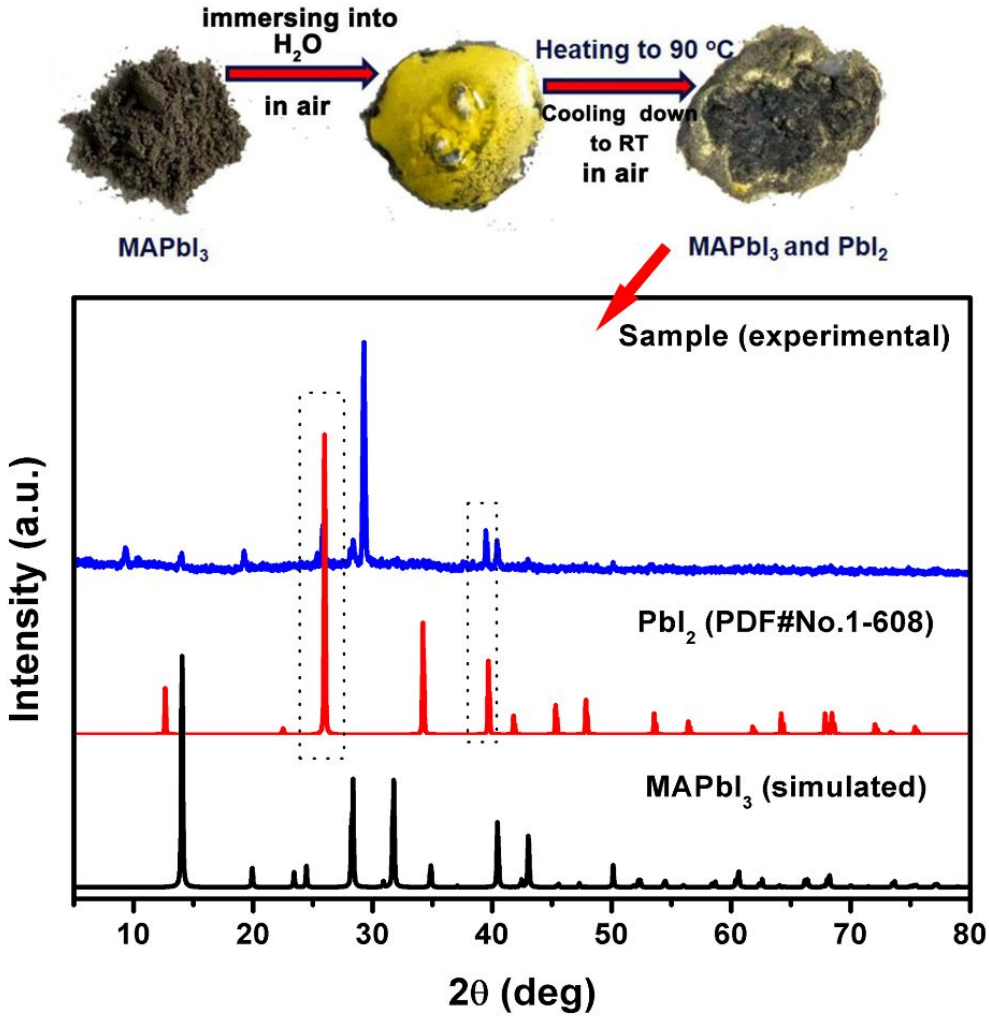

Figure S14. Transformation processes of $MAPbI_3$ single-crystalline grinding powder samples immersing in H_2O and then heating to 90 °C and cooling down to room temperature in air, which was verified to be $MAPbI_3$ and PbI_2 mixtures.

Table S1. Crystal data and structure refinements for $Pb(SCN)_2$ and $MA_2Pb(SCN)_2I_2$ at 293(2) K

Empirical formula	$Pb(SCN)_2$[a]	$(CH_3NH_3)_2Pb(SCN)_2I_2$[b]
Actual formula	$Pb(SCN)_2$	$(CN)_2Pb(SCN)_2I_2$
Formula weight/ $g \cdot mol^{-1}$	323.35	629.19
Temperature/K	293(2) K	
Wavelength/Å	0.71073	
Crystal color	Colorless	Dark red
Crystal system	Monoclinic	Orthorhombic
Space group	*C2/c* (no. 15)	*Pmn2₁* (no. 31)
a/Å	9.6575(4)	18.5640(15)
b/Å	6.5439(3)	6.2639(4)
c/Å	8.2514(4)	6.4739(4)
α/°	90.00	90.00
β/°	92.266(2)	90.00
γ/°	90.00	90.00
Volume/$Å^{-3}$	521.06(4)	752.80(9)
Crystal size (mm^3)	0.2×0.15×0.1	0.12×0.1×0.05
Z	4	2
Density/$g \cdot cm^{-3}$	4.122	2.776
μ(mm^{-1})	33.030	15.555
F (000)	560	544
GOF on F^2	1.200	1.077
Absolute Flack Factor	---	0.298(10)
Absorption correction	Semi-empirical from equivalents	
Refinement method	Full-matrix least-squares on F^2	
Data/restraints/parameters	606/0/34	1761/1/65
R_1, wR_2 [I > 2σ (I)]	0.0637, 0.1716	0.0325, 0.0805
R_1, wR_2 (all data)	0.0638, 0.1717	0.0338, 0.0812
Min/Max Δρ /e$Å^{-3}$	-6.847/5.525	-1.28/2.09
CCDC	1940636	1940635
Growth method	Slow evaporation method (THF or DMF)	Solid-state method

[a] $w=1/[s^2(Fo^2)+(0.1334P)^2+0.0000P]$ where $P=(Fo^2+2Fc^2)/3$

[b] $w=1/[s^2(Fo^2)+(0.0201P)^2+9.5216P]$ where $P=(Fo^2+2Fc^2)/3$

Table S2. Crystal data and structure refinements for $MA_2Pb(SCN)_2I_2$ at 293(2) K

Empirical formula	$(CH_3NH_3)_2Pb(SCN)_2I_2$[a]	$(CH_3NH_3)_2Pb(SCN)_2I_2$[b]	$(CH_3NH_3)_2Pb(SCN)_2I_2$[c]
Actual formula	$(N)_2Pb(SCN)_2I_2$	$(N)_2Pb(SCN)_2I_2$	$(N)_2Pb(SCN)_2I_2$
Formula weight/ g·mol^{-1}	605.17	605.17	605.17
Temperature/K		293(2) K	
Wavelength/Å		0.71073	
Crystal color	Dark red	Dark red	Dark red
Crystal system	Orthorhombic	Orthorhombic	Orthorhombic
Space group	*Pmn2$_1$* (no. 19)	*Pmmn* (no. 59)	*Pmmn* (no. 59)
a/Å	18.5818(18)	6.4675(3)	18.5641(5)
b/Å	6.2690(6)	18.5799(8)	6.4716(2)
c/Å	6.4733(6)	6.2629(2)	6.26520(10)
α/°	90.00	90.00	90.00
β/°	90.00	90.00	90.00
γ/°	90.00	90.00	90.00
Volume/Å^{-3}	754.07(12)	752.58(5)	752.70(3)
Crystal size (mm^3)	0.25×0.1×0.068	0.12×0.08×0.05	0.1×0.08×0.05
Z	2	2	2
Density/g·cm^{-3}	2.665	2.671	2.670
μ(mm^{-1})	15.523	15.553	15.551
F (000)	520	520	520
GOF on F^2	1.116	1.326	1.282
Absolute Flack Factor	0.136(11)	---	---
Absorption correction		Semi-empirical from equivalents	
Refinement method		Full-matrix least-squares on F^2	
Data/restraints/parameters	1355/1/56	974/0/38	972/0/38
R_1, wR_2 [I > 2σ (I)]	0.0376, 0.1123	0.0586, 0.1590	0.0582, 0.1618
R_1, wR_2 (all data)	0.0388, 0.1130	0.0598, 0.1598	0.0621, 0.1651
Min/Max Δρ /eÅ^{-3}	-0.916/2.026	-3.743/3.897	-3.628/3.011
CCDC	1939379	1939377	1939378
Growth method	Slow evaporation method (THF)	Anti-solvent diffusion method (THF/Et_2O)	Anti-solvent diffusion method (THF/Toluene)

[a] $w=1/[s^2(Fo^2)+(0.0674P)^2+4.4575P]$ where $P=(Fo^2+2Fc^2)/3$

[b] $w=1/[s^2(Fo^2)+(0.0316P)^2+30.3281P]$ where $P=(Fo^2+2Fc^2)/3$

[c] $w=1/[s^2(Fo^2)+(0.0499P)^2+25.7378P]$ where $P=(Fo^2+2Fc^2)/3$

Table S3. Crystal data and structure refinements for $MA_2Pb(SCN)_2I_2$ at 190 K and 363 K

Empirical formula	$(CH_3NH_3)_2Pb(SCN)_2I_2$[a]	$(CH_3NH_3)_2Pb(SCN)_2I_2$[b]
Acutal formula	$(CH_3NH_3)_2Pb(SCN)_2I_2$	$(N)_2Pb(SCN)_2I_2$
Formula weight/ g·mol^{-1}	641.29	605.17
Temperature/K	190 K	363 K
Wavelength/Å	0.71073	
Crystal color	Dark red	Black
Crystal system	Orthorhombic	Orthorhombic
Space group	*Pmn2$_1$* (no. 31)	*Pmmn* (no. 59)
a/Å	18.3886(8)	6.4409(5)
b/Å	6.2412(3)	18.8578(13)
c/Å	6.4624(2)	6.2954(4)
α/°	90.00	90.00
β/°	90.00	90.00
γ/°	90.00	90.00
Volume/Å^{-3}	741.67(5)	764.65(9)
Crystal size (mm^3)	0.1×0.08×0.05	0.1×0.08×0.05
Z	2	2
Density/g·cm^{-3}	2.872	2.628
μ(mm^{-1})	15.790	15.308
F (000)	568	520
GOF on F^2	0.947	1.196
Absolute Flack Factor	0.088(7)	---
Absorption correction	Semi-empirical from equivalents	
Refinement method	Full-matrix least-squares on F^2	
Data/restraints/parameters	1316/1/67	2445/0/110
R_1, wR_2 [I > 2σ (I)]	0.0228, 0.0421	0.0551, 0.1620
R_2, wR_2 (all data)	0.0277, 0.0442	0.0563, 0.1631
Min/Max Δρ /eÅ^{-3}	-0.841/ 0.647	-2.758/ 3.890
CCDC	1939376	1939380

[a] $w=1/[s^2(Fo^2)+(0.00P)^2+ 0.00P]$, where $P=(Fo^2+2Fc^2)/3$
[b] $w=1/[s^2(Fo^2)+(0.0824P)^2+ 9.4420P]$where $P=(Fo^2+2Fc^2)/3$

REFERENCES

(1) Dang, Y.; Liu, Y.; Sun, Y.; Yuan, D.; Liu, X.; Lu, W.; Liu, G.; Xia, H. and Tao, X. Bulk crystal growth of hybrid perovskite material $CH_3NH_3PbI_3$, *CrystEngComm* **2015**, *17*, 665-670.

(2) Dang, Y.; Zhou, Y.; Liu, X.; Ju, D.; Xia, S.; Xia, H. and Tao, X. Formation of hybrid perovskite tin iodide single crystals by top-seeded solution growth, *Angew. Chem. Int. Ed.* 2016, *55*, 3447-3450; *Angew. Chem.* **2016**, *128*, 3508-3511.

(3) Dang, Y.; Liu, X.; Sun, Y.; Song, J.; Hu, W. and Tao, X., Bulk chiral halide perovskite single crystals for active circular dichroism and circularly polarized luminescence, *J. Phys. Chem. Lett.* **2020**, *11*, 1689-1696.

(4) Dang, Y.; Zhong, C.; Zhang, G.; Ju, D.; Wang, L.; Xia, S.; Xia, H. and Tao, X. Crystallographic investigations into properties of acentric hybrid perovskite single crystals $NH(CH_3)_3SnX_3$ (X = Cl, Br), *Chem. Mater.* **2016**, *28*, 6968-6974.

(5) Dang, Y.; Wei, J.; Liu, X.; Wang, X.; Xu, K.; Lei, M; Hu W. and Tao, X. Layered hybrid perovskite solar cells based on single-crystalline precursor solutions with superior reproducibility, *Sustainable Energy Fuels*, **2018**, *2*, 2237-2243.

(6) Dolomanov, O.V.; Bourhis, L. J.; Gildea, R. J.; Howard J. A. K. & Puschmann, H. OLEX2: a complete structure solution, refinement and analysis program, *J. Appl. Cryst.* **2009**, *42*, 339-341.

(7) Spek, A. L. Structure validation in chemical crystallography, *Acta Cryst.* **2009**, *D65*, 148-155.

(8) Sheldrick, G. M. Crystal structure refinement with SHELXL, *Acta Cryst.* **2015**, *C71*, 3-8.

(9) Wendlandt, W. M.; Hecht, H. G. *Reflectance Spectroscopy*; Interscience: New York, **1966**; p62.